Article

The Influence of Voltage on Gliding Arc Discharge Characteristics, the Composition of Air Plasma, and the Properties of BG-11 Medium

Liutauras Marcinauskas [1,2,*], Žydrūnas Kavaliauskas [1], Kamilė Jonynaitė [3], Rolandas Uscila [1], Mindaugas Aikas [1], Skirmantas Keršulis [3], Antanas Strakšys [3], Arūnas Stirkė [3] and Voitech Stankevič [3]

[1] Plasma Processing Laboratory, Lithuanian Energy Institute, Breslaujos Str. 3, 44403 Kaunas, Lithuania; zydrunas.kavaliauskas@lei.lt (Ž.K.); rolandas.uscila@lei.lt (R.U.); mindaugas.aikas@lei.lt (M.A.)

[2] Department of Physics, Kaunas University of Technology, Studentu Str. 50, 51368 Kaunas, Lithuania

[3] Department of Functional Materials and Electronics, State Research Institute, Center for Physical Sciences and Technology, Savanoriu Ave. 231, 10257 Vilnius, Lithuania; kamile.jonynaite@ftmc.lt (K.J.); skirmantas.kersulis@ftmc.lt (S.K.); antanas.straksys@ftmc.lt (A.S.); arunas.stirke@ftmc.lt (A.S.); voitech.stankevic@ftmc.lt (V.S.)

* Correspondence: liutauras.marcinauskas@lei.lt

Abstract: A gliding arc discharge (GAD) plasma device has been developed and tested. Possible applications areas for GAD plasma could be microalgae suspension treatments and the creation of plasma-activated water. To understand its behavior, the influence of the input power on the electrical characteristics of the generated GAD plasma was investigated using an oscilloscope. The waveforms of the voltage and current of GAD plasma are presented. The duration of the discharge time and the evolution of the arc during discharge were determined and investigated. It was revealed that the increase in the output voltage prolonged the duration of the arc discharge. The composition of the air plasma was investigated using a flame-emission spectrometer and acousto-optic emission spectrometer. It was revealed that the main species in the emission spectra of the GAD air plasma were N_2, N_2^+, N^+, NO, and O species. Furthermore, the increase in the input power enhanced the ionization degree of the air plasma and increased the intensities of the emission lines associated with N_2^+, NO, and O species. An increase in the conductivity of the BG-11 medium was observed. Physicochemical analyses of the plasma-activated BG-11 medium indicated an increase in the concentration of nitrite and nitrate ions and hydrogen peroxide with an enhancement of the voltage.

Keywords: gliding arc discharge; air plasma; emission spectra; nitrogen; plasma-activated medium; hydrogen peroxide

1. Introduction

In recent years, there has been a drastic increase in research related to the development of novel atmospheric non-thermal or thermal plasma systems and application of plasma in the medicine and agricultural fields for the treatment of seeds or plants, the creation of plasma-activated water, the cleaning of wastewater, etc. [1–8]. It was demonstrated that the treatment of seeds with plasma improves their quality and germination rates, leading to enhanced crop yields [4,7,8]. Plasma also was successfully used to irradiate various types of algae in order to improve the extraction yield of valuable compounds or promote algae growth [2,3].

The gliding arc discharge (GAD) plasma setup stands out as one of the most widely used methods for plasma generation. The main advantages of GAD plasma compared to other non-thermal plasmas are its high processing efficiency, high electron temperature and density, simple configuration, and the easy control of its process parameters [8–20]. It has been observed that GAD plasma is very widely used for plasma reforming and

fuel and waste treatment [12–16], and it could be also used for bacterial inactivation and food decontamination [10,17–20], the creation of plasma-activated water [5,8,21], and surface treatments and modifications [22–26]. Gliding arc discharge characteristics such as current and voltage values, the arc column length, discharge duration, density, and type of species produced in the plasma are strongly affected by the geometry and configuration of the electrodes, the experimental parameters, and the type of gas used for the plasma's generation [13,16,18,20]. It should be noted that for the application of GAD plasma in the creation of plasma-activated water and the treatment of seeds, plants, or microalgae, the elemental composition of the plasma and the type of species produced play a crucial role [3,8,19–21]. The authors of previous studies observed that plasma-irradiated liquids had higher conductivity values [4,6,8,21]. Meanwhile, the main ions and radicals which are produced in water or various liquids after plasma treatment are nitrate, nitrite, nitrogen dioxide, and hydrogen peroxide [4,6,8]. Therefore, the pH values, conductivities, and amount of the various species in these liquids depended not only on the type of liquids, but also on the type of gases used, plasma treatment times, the type of discharge, etc. [4,6,8,21].

Optical emission spectroscopy (OES) is a widely used technique to determine the main species in various atmospheric plasmas [4,6,21,27–35]. Air, oxygen, nitrogen, and oxygen–nitrogen gas mixtures are widely used for plasma formation in order to create reactive oxygen and nitrogen species, which are considered to be the main agents inducing structural, chemical, or biological changes in the plasma treatment of water and seeds [4,6,8,19–21,27,28,31]. The intensity of the emission lines is related to the density of the species produced in the plasma. The variation of the process parameters (applied voltages, frequency, used gas flow rate, type of gas, etc.) has a strong influence on the composition and densities of the species produced in the plasma [6,19,22,27–29,35]. It was determined that the typical emission spectra of air plasma produced by a gliding arc discharge had spectral lines related to the excited states of NO, OH, NH, N_2, N_2^+, and O species [19–21,26]. The variation of the discharge power and air flow rate allows us to increase or reduce the density of the dominant species in an air plasma [20,35]. M. Parker et al. [35] found that an increase in the air flow rate from 14 SLM to 42 SLM increased the intensities of the exited NO_γ, OH, and N_2 species in the plasma. I. Muzammil et al. [34] observed that the intensity of the emission lines related to NO, N_2^+, and N_2 was enhanced with a reduction of the air flow rate from 150 L/min to 20 L/min. S.H.M. Ashtiani et al. [20] demonstrated that the N_2, N_2^+, and OH species were dominant in air plasma, while the intensity of the O and NO emission lines was very low, and that the optimal treatment time of grape seeds was from 40 to 60 s. J. Pawłat et al. [21] observed that the GAD plasma produced using a mixture of N_2/O_2 gases was a strong source of nitrogen oxides (NO and NO_2), while the dominant species in its emission spectra were N_2 particles. The variation in the gas composition also had an influence on the plasma's temperature. P. Dimitrakellis et al. [26] indicated that the dominant particle in their GAD plasma was N_2, with low amount of NO and OH species. P. Dimitrakellis et al. [31] observed that the intensity of the atomic oxygen lines in air plasma was very low due to the rapid dispersal of the exited atomic oxygen. X.Q. Wang et al. [33] observed that the dominant species in DBD air plasma were N_2 and N_2^+, while the intensity of the emission lines related to the NO and atomic oxygen species was very low, indicating that the amount of oxygen species in the plasma was very low. Therefore, to successfully use gliding arc discharge plasma for the irradiation of plants or algae, it is important to determine the optimal discharge parameters and to estimate the composition of the used plasma. It is also important to determine the relationship between the composition of the plasma and the discharge parameters (voltage, frequency, gas flow rate, etc.).

The main aims of this work were to create a gliding arc discharge plasma device to investigate the arc evolution over time at various output voltages, to identify the main species produced in GAD air plasma and to determine the influence of the voltage on the emission spectra of the air plasma. Additionally, the influence of plasma irradiation on

the physical and chemical parameters of BG-11 freshwater microalgae growth medium was investigated.

2. Materials and Methods

The experimental set-up, with a gliding arc discharge plasma reactor, was developed at the Lithuanian Energy Institute. A schematic view of the gliding arc discharge (GAD) plasma set-up is presented in Figure 1. The constructed plasma set-up includes the plasma reactor and power supply including the variable frequency and voltage generator (AC Power) and high-voltage transformer (Figure 1) and air supply systems. The air supply system includes a compressor, mass flow controllers, metal tubes, plastic pipes, and steel connections. Compressed air was used as the plasma-forming gas. The air was injected into the plasma reactor at room temperature from the top of the electrodes, with a flow rate of 13.39 L/min, and tangentially, with a flow rate of 9.44 L/min, before applying a high voltage. This combination of air flow rates made it possible to obtain the same temperature in the plasma over the entire surface area of the Petri dish. Flowmeters were used to control and maintain a stable air flow rate during the discharge process. The G2000 high voltage/medium frequency generator (Redline Technologies Elektronik GmbH, Baesweiler, Germany) was used to generate the gliding arc discharge at atmospheric pressure. Discharge voltages were obtained using a Rigol DS4012 oscilloscope (Rigol Technologies, Inc. Suzhou, China) with a high-voltage passive probe, Tektronix P6015A (Tektronix, Co., Ltd. Shanghai, China). The current during discharge was measured with a current probe, Pintek PA-699 (Pintek Electronics Co., Ltd. New Taipei City, Taiwan). Two "knife-like" electrodes with a length of 52 mm and width of 25 mm were used, and the gap between the electrodes at the top was kept at 1 mm. The output voltage (V_G) of the AC generator was changed from 50 V up to 250 V keeping the frequency at 270 kHz and the signal duty cycle at 0.35 during discharge. The turn ratio of high-voltage transformer was 1:33.
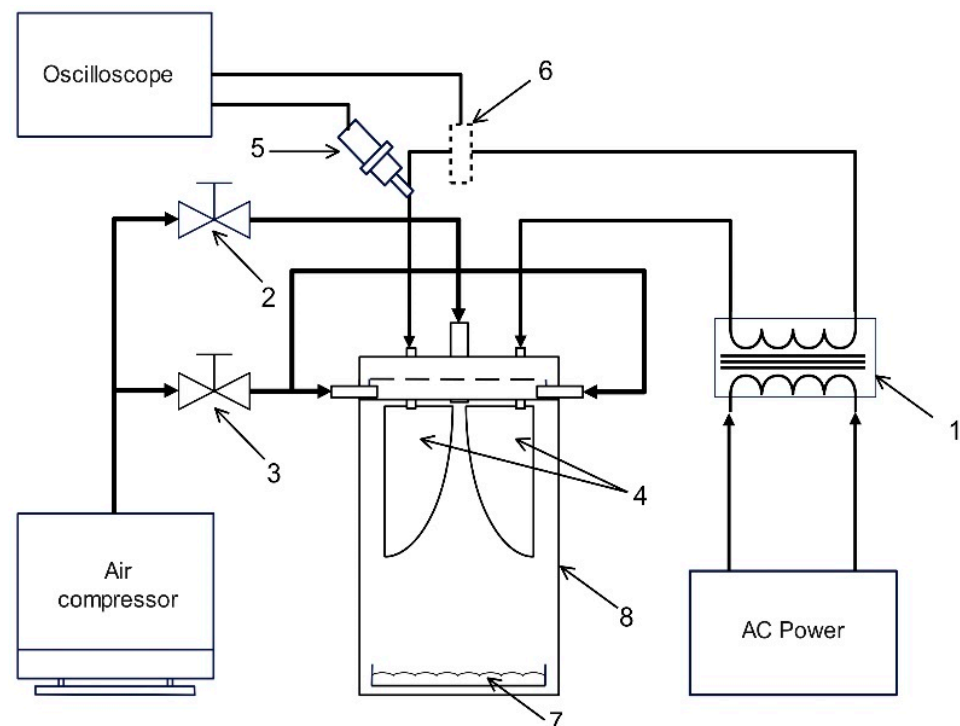
Figure 1. A schematic view of the GAD plasma system. 1—high-voltage transformer; 2, 3—air flowmeter controllers; 4—electrodes; 5—high-voltage probe; 6—current probe; 7—Petri dish with BG-11 medium; 8—plasma reactor.

Determination of the evolution and duration of the arc discharge was performed by analyzing the slow-motion images captured by a high-speed camera (Phantom Miro M310, Wayne, NJ, USA). A fast, ~5260 frames per second, 12-bit, 25.6 mm × 16.0 mm CMOS sensor camera composed of a zoom lens and a neutral UV filter was used to visualize the gliding arc distributions at various voltages.

The emission spectra of the air plasma were measured using a flame-emission spectrometer, Flame UV-VIS (Ocean Insight, Orlando, FL, USA), in a wavelength range of 200–1000 nm. The integration time was 0.375 s, the number of accumulated scans was 10, and each air plasma spectrum was measured 3 times to calculate its average value. Also, air plasma composition was determined using an acousto-optic emission spectrometer, IFU AOS4 (in the range of 250–800 nm), which operates based on a tunable acousto-optical filter (AOTF). The spectrometer had a solid-state monochromator/grating (with a spectral resolution: 0.05 nm at 250 nm and 0.5 nm at 800 nm). The emission spectra of the air plasma were measured in the area between the electrodes, at 35 mm from the top, and a total of 3 scans were performed.

In order to evaluate the effect of the developed plasma generator, BG-11 freshwater microalgae growth medium was chosen as a test sample, and was collected after 7 days of the *Chlorella vulgaris* cultivation process [36]. Changes in the physical (temperature, conductivity) and chemical (radical composition) properties of the medium were monitored before and after treatment with a wide range of plasma voltages and a treatment duration of 5 min. During the experiment, 10 mL of BG-11 medium was injected in a Petri dish located in a position 30 mm below the electrodes. During the plasma processing of the medium, temperature variations were measured using two chromel-aliumel thermocouples. The thermocouples were immersed into the BG-11 medium near the surface. The temperature data presented in this study are the average value of both thermocouples. It should be noted that the temperature of the sample dropped immediately after it was removed from the treatment chamber. Therefore, its pH and electrical conductivity were determined 5 min after treatment, without temperature compensation, using a Orion 720Aplus (Thermo Scientific™, Waltham, MA, USA) and conductivity meter with an InLab 738-ISM probe (Mettler Toledo, Oakland, CA, USA). The nitrate and nitrite concentration in the suspension before and after treatment were determined using commercial tests (Merck KGaA, Darmstadt, Germany) according to the manufacturer's protocol. The concentrations of hydrogen peroxide in the samples were calculated from their iodine values [37]. An iodine calibration curve was constructed by dissolving iodine in isopropanol to a final concentration of 10 mM. The amount of iodine solution taken was diluted with medium (1 M acetic acid–2.5 M KJ–H_2O = 10:0.5:1) to give iodine concentrations from 0.2 mM to 1 mM, and its optical density at 450 nm was measured. The peroxide content of the sample was measured by mixing 1 mL of the sample with 5 mL of 1 M acetic acid and 0.5 mL of 2.5 M KJ and leaving it in the dark for 5 min. The optical density at 450 nm was then measured and the iodine concentration was calculated from the calibration curve.

3. Results and Discussions

The electric characteristics of the gliding arc discharge were obtained by determining the waveforms of the voltage and discharge arc current in the air plasma. The electrical characteristics were measured by changing the output voltage from 50 V to 250 V. The typical voltage and current waveforms of the GAD in air plasma are presented in Figure 2. The voltage waveform is a serrate-like shape, which is due to the periodic change in the length of the arc column over time. The arc current also increases slightly as the arc length increases (Figure 2a,c). It should be noted that, with the increase in the output voltage of voltage generator from 50 V to 250 V, the arc column becomes longer, and both the voltage and current waveform last longer [20,38]. Similar behaviors of the voltage and current waveforms were obtained for different gliding arc discharges [13,16,20].
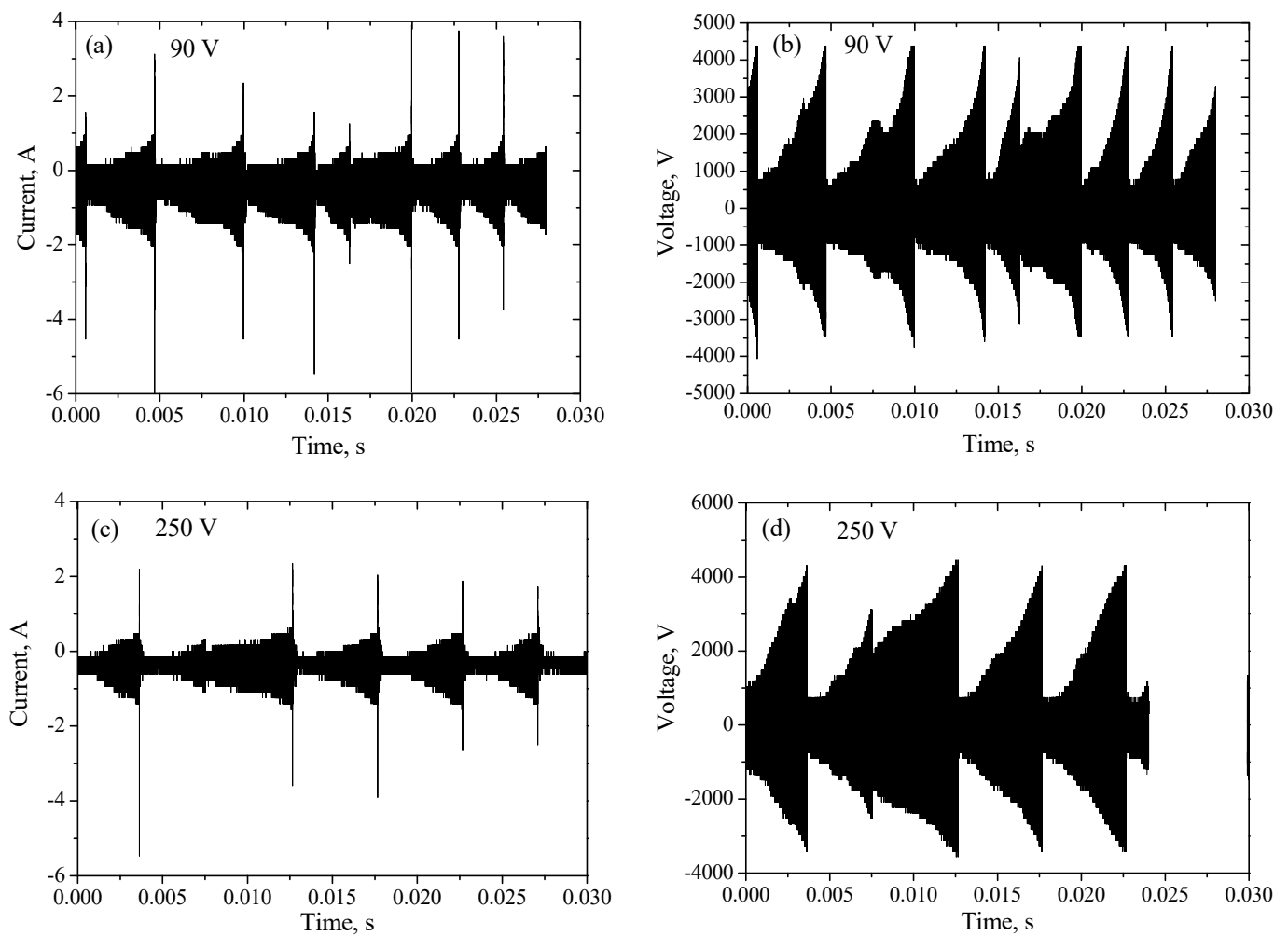
Figure 2. Waveforms of current (**a**,**c**) and voltage (**b**,**d**) for the GAD discharge with a V_G of 90 V (**a**,**b**) or 250 V (**c**,**d**).

The voltage increases to its maximum value as the gliding arc column is elongated. The arc breakdown occurs when the distance between the electrodes becomes too long and the applied electric field is too low to sustain the discharge. The voltage drops very rapidly and the arc current rises instantly as the breakdown occurs (Figure 2). The growing arc requires more power or a higher voltage to sustain itself, as the air/gas breakdown voltage depends on the gap distance between the electrodes (*d*) and the pressure (*p*), according to Paschen's law. The *pd* value is enhanced with the increase in the arc length, and at the critical arc length the voltage becomes insufficient to sustain the elongation of the discharge [9]. It should be noted that the duration of the discharge, the voltage, and current values depend on the shape of the electrodes as well as on the flow rate of the gases and the voltage values [13,16,20,38]. However, the shape and period of the waveforms were slightly different even when the output voltage was kept constant (Figure 2b). With the increase in the voltage, the electric field is increased, and the arc propagates and reaches further distances (Figures 2 and 3) [38].

In order to determine the evolution of the arc during the discharge a high-speed camera was used. The images of the arc's evolution in air plasma at various V_G values are presented in Figures 3 and 4. These images were also used to determine the discharge duration and compared with the data obtained from the voltage and current waveforms.
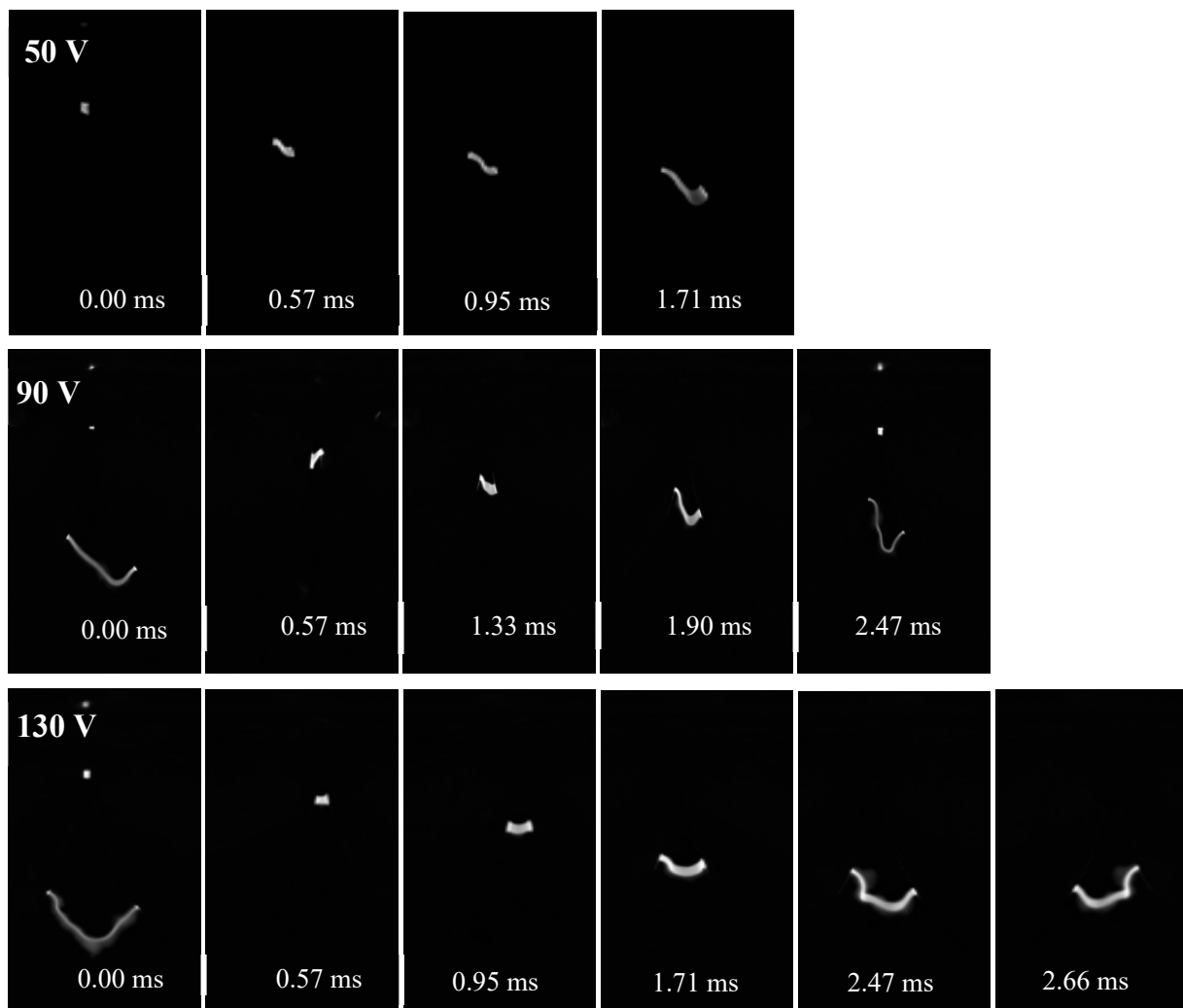
Figure 3. Photo images showing the arc evolution over time at 50 V, 90 V, and 130 V voltages.

It can be seen that the arc is ignited at the minimum gap between the electrodes and that the carrier air pushes the arc forward. The voltage increases with the movement of the arcs through the electrodes and as they increase in length (Figures 2 and 4). When the arc reaches its maximum length, the arc breaks up and is immediately reignited at the point of the smallest gap, and then the arc glides further (Figure 4, see the first or last photo images). With the increase in the voltage, the plasma volume and length become greater (Figure 5). The visual increase in the plasma volume and area can be clearly seen from the photo images in Figure 5. The higher voltage can support the arc running across a higher resistance (larger gap). The increase in current values versus time with the expansion of arc could be due to fact that the voltage increases faster than the resistance between the electrodes.

The average values of the life-time of the arc discharge, determined from the electric characteristics and the images taken by a high-speed camera, are presented in Figure 6. It was found that the average discharge duration was 1.71 ± 0.29 ms when a voltage of 50 V was used. The average discharge duration slightly increased, up to ~2.95 ± 0.35 ms, when the V_G was set to 90 V. It should be noted that the increase in the voltage from 50 V to 250 V increased the arc discharge duration almost linearly, up to 5.21 ± 0.61 ms (Figure 6). It was determined that the arc velocity gradually decreased as the arc glided along the electrodes, mainly due to the reduction of the driving force as the gas flow velocity is lower at a longer distance [38]. Thus, it could be concluded that the duration of the discharge was highly
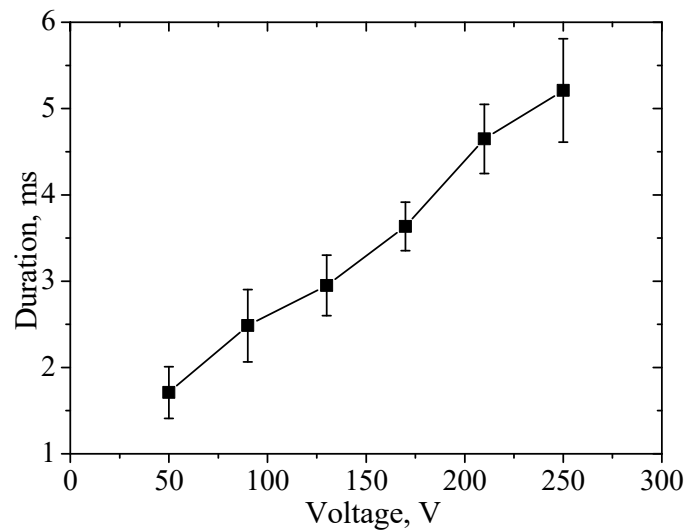
dependent on the output voltage and could be enhanced up to three times with an increase in the voltage.
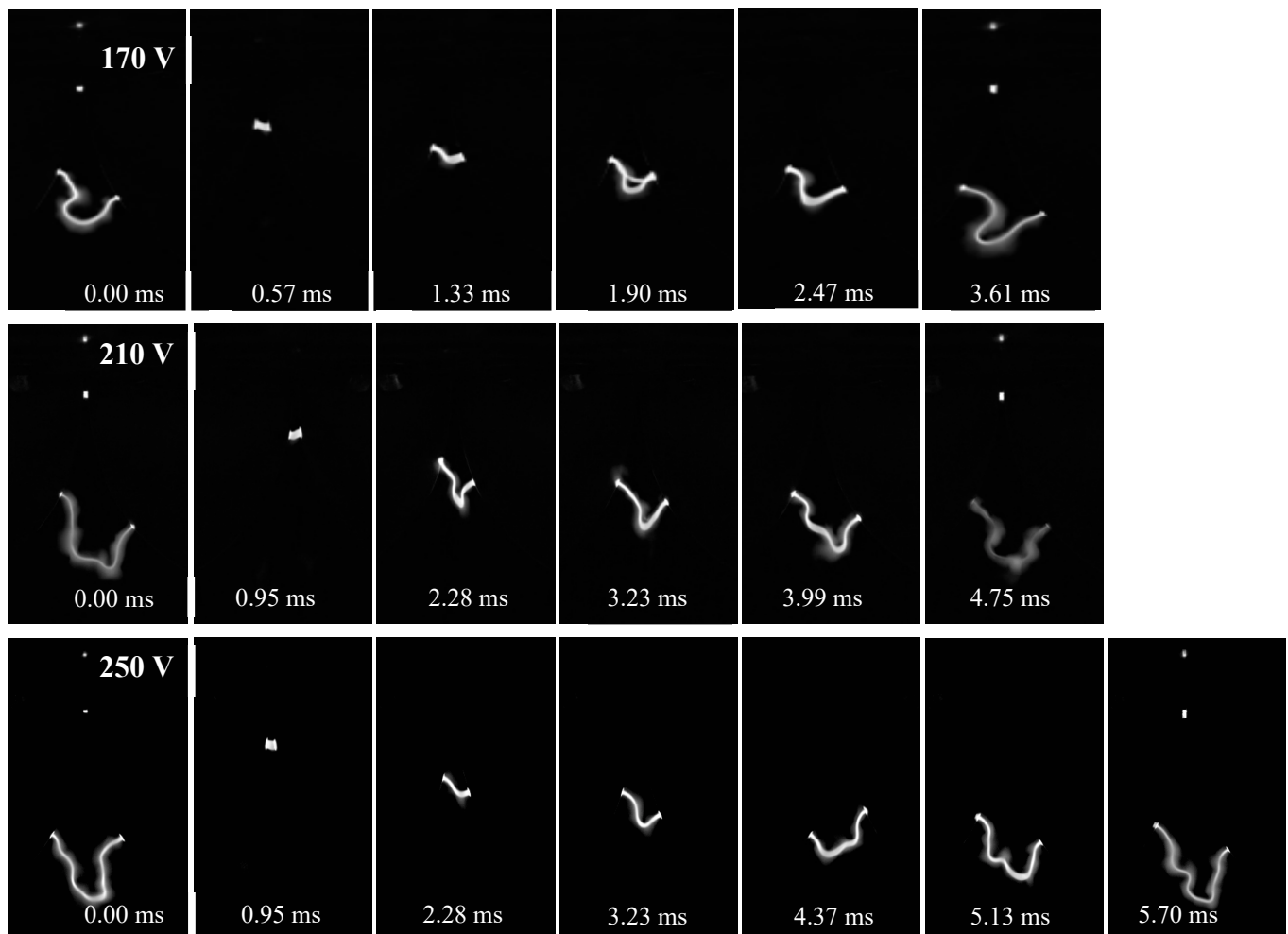
**Figure 4.** Photo images of arc evolution over time in air plasma at higher V_G values.
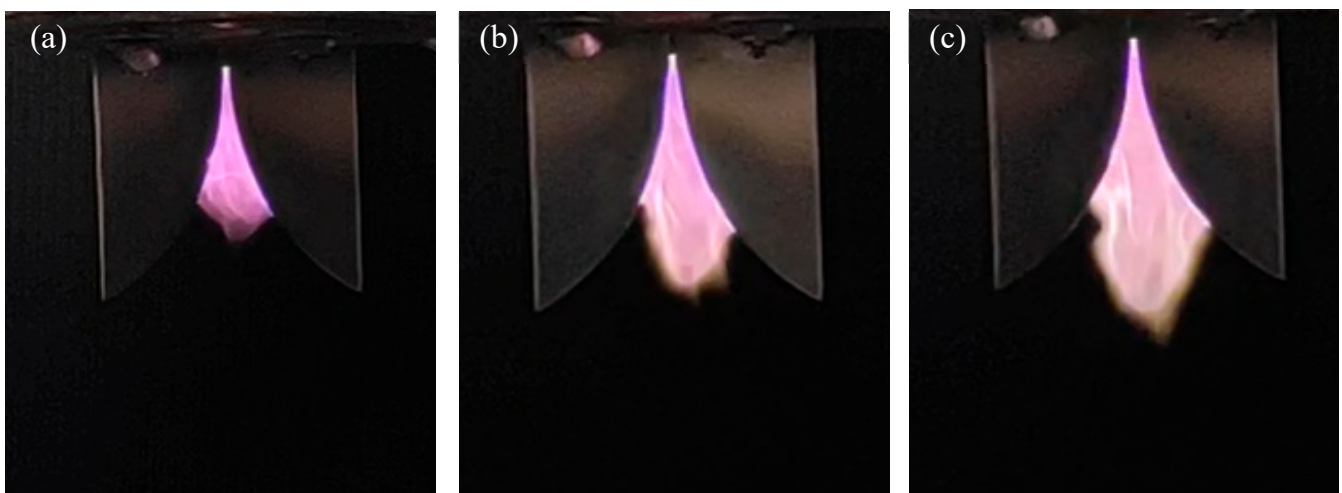
Figure 5. Photo of the GAD plasma when V_G was set at (**a**) 90 V, (**b**) 170 V, and (**c**) 250 V.

Figure 6. Variation of gliding arc discharge duration versus output voltage.

The optical emission spectrum of the air plasma produced using a gliding arc discharge at $V_G = 250$ V is given in Figure 7. The emission spectrum offers us information about the type of excited species existing in the air plasma. It was observed that the main particles in the air plasma were exited nitrogen molecules. The highest intensity peaks observed at 316 nm, 337 nm, 353 nm, 358 nm, and 379 nm are attributed to the (0, 1), (0, 0), (2, 1), (1, 0), and (2, 0) N_2 vibrational modes, respectively [6,11,22]. The appearance of peaks in the range of the 280–450 nm wavelengths is related to the various vibrational mode transitions of the second positive system of N_2 in the air plasma [6,15,22,39–41]. It was established that the highest intensity emission peaks in the range of 280–430 nm are attributed to the second positive system of N_2 ($C^3\Pi_u \rightarrow B^3\Pi_g$) and the first negative system of N_2^+ ($B^2\Sigma^+_u \rightarrow X^2\Sigma^+_g$), which are usually obtained in air or nitrogen plasmas [6,11,15,21,22,31].
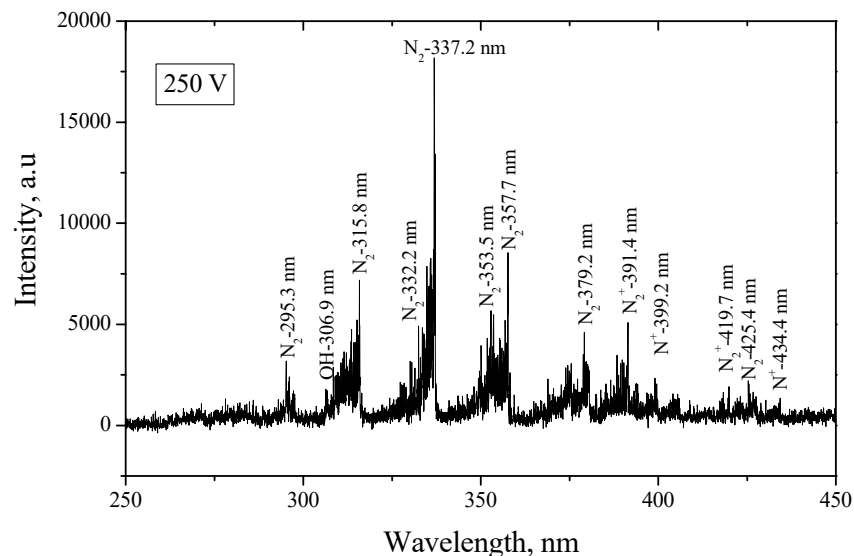

Figure 7. Optical emission spectrum of air plasma when the output voltage was 250 V.
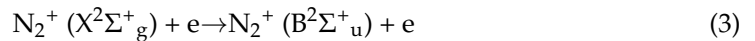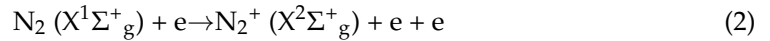
The low-intensity emission peaks at 391 nm, 419 nm, and 470 nm are attributed to the first negative band of the molecular nitrogen ion (N_2^+) (Figure 7). The N_2 molecules react with the plasma electrons through direct impact; part of the electrons' energy is transferred to the molecule and the excitation or ionization of N_2 proceeds. It was determined that the formation of N_2^+ in air plasma can be attributed to the direct electron-impact ioniza-

tion of the nitrogen molecules from their ground state $(X^1\Sigma_g^+)v'_{=0}$ to N_2^+ excited states $(B^2\Sigma_u^+)v''_{=0}$ via the following reaction:

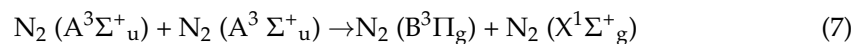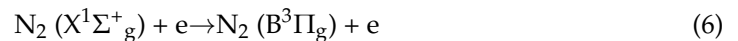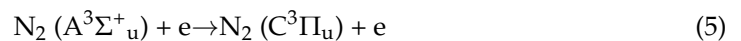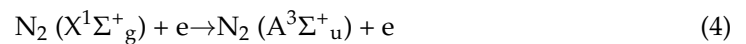$$N_2 \ (X^1\Sigma^+_g) + e \rightarrow N_2^+ \ (B^2\Sigma^+_u) + e + e \tag{1}$$
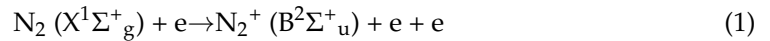
Another way to produce a molecular nitrogen ion (N_2^+) is a two-step ionization process via the following reactions:

$$N_2 \ (X^1\Sigma^+_g) + e \rightarrow N_2^+ \ (X^2\Sigma^+_g) + e + e \tag{2}$$

$$N_2^+ \ (X^2\Sigma^+_g) + e \rightarrow N_2^+ \ (B^2\Sigma^+_u) + e \tag{3}$$

Firstly, due to electron collisions with the nitrogen molecule, ionization takes place and the N_2 molecule moves from its ground state to a molecular nitrogen ion (N_2^+) ground state (Equation (2)). In the second step, the transition from the N_2^+ ground state to the N_2^+ excited state takes place due to the excitation induced by the electron impact (Equation (3)).

The main reaction for the production of excited nitrogen molecules could be related to the collisions of nitrogen molecules with electrons [4,6,15]:

$$N_2 \ (X^1\Sigma^+_g) + e \rightarrow N_2 \ (A^3\Sigma^+_u) + e \tag{4}$$

$$N_2 \ (A^3\Sigma^+_u) + e \rightarrow N_2 \ (C^3\Pi_u) + e \tag{5}$$

$$N_2 \ (X^1\Sigma^+_g) + e \rightarrow N_2 \ (B^3\Pi_g) + e \tag{6}$$

$$N_2 \ (A^3\Sigma^+_u) + N_2 \ (A^3 \ \Sigma^+_u) \rightarrow N_2 \ (B^3\Pi_g) + N_2 \ (X^1\Sigma^+_g) \tag{7}$$

After the collision of electrons with nitrogen molecule, the excited N_2 molecule is formed (a transition from the ground state $(X^1\Sigma^+_g)$ to the excited state $(A^3\Sigma^+_u)$ occurs) (Equation (4)). Its transition from the exited state of $A^3\Sigma^+_u$ to the $C^3\Pi_u$ state is generated by nitrogen molecules collisions with electrons (Equation (5)). Meanwhile, the formation of nitrogen molecules with excited states of $(B^3\Pi_g)$ is via the reactions (6) and (7).

The low-intensity peak at 306.9 nm in the emission spectrum is attributed to the OH radical (Figure 7). It was pointed out that the emission lines attributed to the OH and NO species are usually obtained in air plasmas in UV region [11,39]. The appearance of the OH radical is due to the existence of water vapor in the ambient air [39]. Thus, the air plasma was additionally measured by a flame-emission spectrometer. The emission spectra obtained at the 90 V and 250 V voltages are presented in Figure 8a,b. Their main peaks were related to exited nitrogen molecules and molecular nitrogen ions (Figure 8a). However, the emission spectra demonstrated a formation of peaks at ~236 nm, 246 nm, 258 nm, and 283 nm, attributed to the exited states of NO_γ species [4,11,32,39].
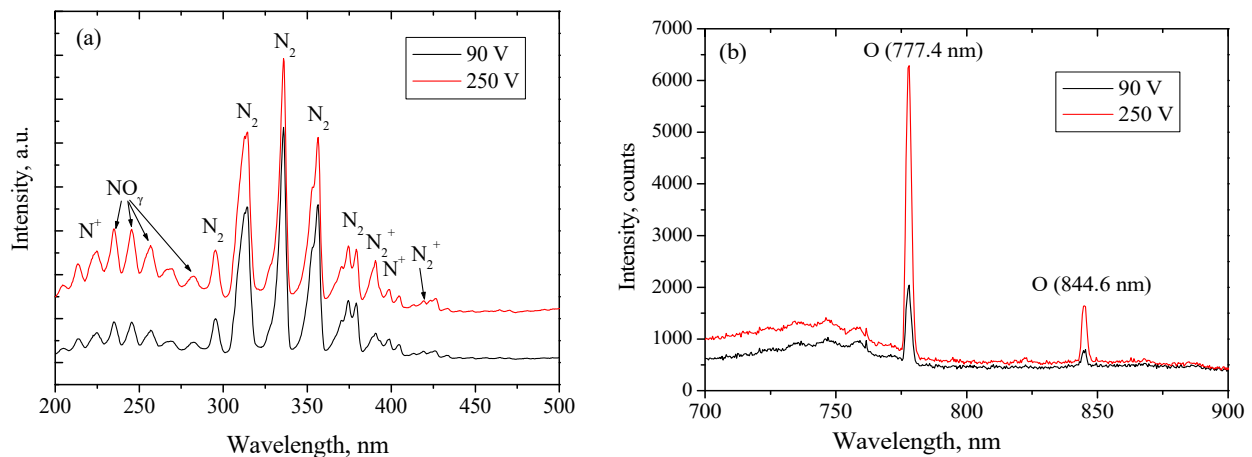
Figure 8. Emission spectra of the air plasma when V_G was 90 V and 250 V.

The existence of the NO β-system ($B^2\Pi - X^2\Pi$) and NO γ-system ($A^2\Sigma^+ - X^2\Pi$) were observed in the wavelength range 200–300 nm for nitrogen or nitrogen–oxygen plasmas [32,39]. The emission lines obtained at the 777.4 nm and 844.6 nm wavelengths are related to the existence of atomic oxygen (O), with transition lines of $3p^5P \rightarrow 3s^5S$ and $3p^3P \rightarrow 3s^3S$, respectively (Figure 8b) [4,19,33,42]. It should be noted that the intensity of the emission line attributed to atomic oxygen at 777 nm was more than two times lower than the intensity of the molecular nitrogen ion (Figure 9).
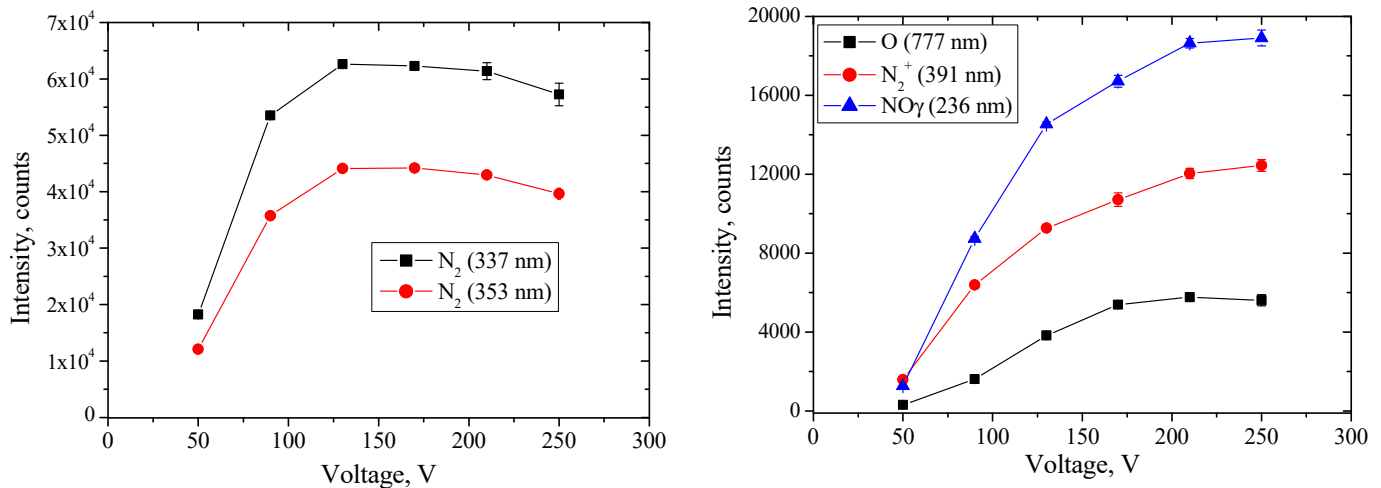
Figure 9. Emission intensities of various species as a function of the output voltage.

The low-intensity peaks in the emission spectra of air plasma at ~221 nm, ~399 nm, and ~434 nm indicate the formation of atomic nitrogen ions (Figures 8 and 9) [6]. It should be noted that several low-intensity emission peaks at 464 nm and 636 nm have been attributed to oxygen ions (O^+) and molecular oxygen ions (O_2^+), respectively [6,42].

The variation of the intensities of the main emission lines of the air plasma were determined and are presented in Figure 9. The variation of the intensity of the peaks related to the exited N_2 species observed at 337 nm and 353 nm versus the applied plasma generator voltage is presented in Figure 9, on the left.

The results indicated that the emission line intensity related to the N_2 exited species at 336 nm increased from 18,200 counts to 62,600 counts with the increase in the V_G from 50 V to 130 V, respectively. The further increase in the voltage up to 250 V resulted in a slight decrease in the intensity values of the N_2 peak at 336 nm. It was found that the intensity of the N_2 emission line was reduced by ~8.5%. Similar dependence trends of intensities versus voltage were obtained for all vibrationally excited N_2 molecules.

The highest intensity of the atomic oxygen peak was obtained at the ~777 nm wavelength. The increase in the voltage from 50 to 210 V increased its peak intensity from 315 counts to 5760 counts. However, the intensity of the emission peak was slightly reduced (by 2.5%) when the highest voltage was used (Figure 9). The intensity of the emission line at 391 nm, attributed to the molecular nitrogen ion (N_2^+), increased with the increase in the voltage. It was observed that the intensity was enhanced 7.8 times with the increase in the voltage from 50 to 250 V. This result indicates that the ionization degree of the plasma was enhanced. The energy of the electrons was enhanced at higher voltages and the possibility of the ionization of the nitrogen molecules increased as well. The slight reduction of the intensities of the emission lines attributed to the exited N_2 species at higher voltages is also a sign that the quantity of the ionization reactions was increased. The intensity of the emission line at 236 nm, assigned to NO_γ, was enhanced from 1300 counts to 18,900 counts with the increase in the voltage from 50 V to 250 V. It was stated that the formation of NO_γ

species in air plasma is due to a reaction between oxygen and nitrogen molecules and a third body (electrons, atoms, or molecules) with a relatively high amount of energy [6].

$$N + O + e \rightarrow NO + e \tag{8}$$

The formation of the NO species in plasmas could also be due to the Zeldovich mechanism, as in Equations (9) and (10) [21]:

$$N + O_2 \rightarrow NO + O \tag{9}$$

$$N_2 + O \rightarrow NO + N \tag{10}$$

It was found that in pure-nitrogen GAD plasma the formation of exited nitrogen molecules has the highest probability of occurring [15]. The emission spectra of the air plasma produced by GAD also demonstrated similar trends (Figures 7 and 8). W. Wang et al. [41] observed that the formation of various NO_x particles very strongly depends on the vibrational excitation of N_2 species. It was established that the intensity of the NO, N_2^+, and N_2 emission lines depended on the air flow rate in GAD [35]. It should be noted that the dominant particles in the GAD air plasma were the reactive nitrogen species N_2, N_2^+, N^+, and NO_γ. Meanwhile, the intensities of the emission lines of the atomic oxygen (O) or oxygen ions (O^+) in air plasma were quite low, which leads us to the conclusion that the densities of those particles in the plasma were significantly lower compared to the nitrogen species. The existence of the reactive nitrogen species and even a small amount of oxygen reactive species in the emission spectra of air plasma produced by GAD shows that the created plasma set-up is suitable for the treatment of algae or seeds and production of plasma-activated water or liquid.

The BG-11 freshwater microalgae growth medium was chosen as a test sample and its physicochemical properties were investigated. The first significant change during the plasma treatment was the increase in the temperature in the medium (Figure 10a), which was recorded when V_G exceeded 130 V. Further increases in the output voltage from 170 V to 250 V increased the temperature of the sample to 46 °C, 49 °C, and 54 °C, respectively. The increase in the temperature is due to the higher ionization degree of the plasma induced at higher voltages. The changes recorded after the plasma treatment included changes in pH, which was initially around 7.5. Increasing the voltage from 90 V to 250 V resulted in a decrease in the medium's pH from 7.37 to 6.99 (Figure 10b). As the plasma generator's voltage was increased, the pH value started to decrease, but a significant decrease (~7%) was only observed at V_G of 250 V.
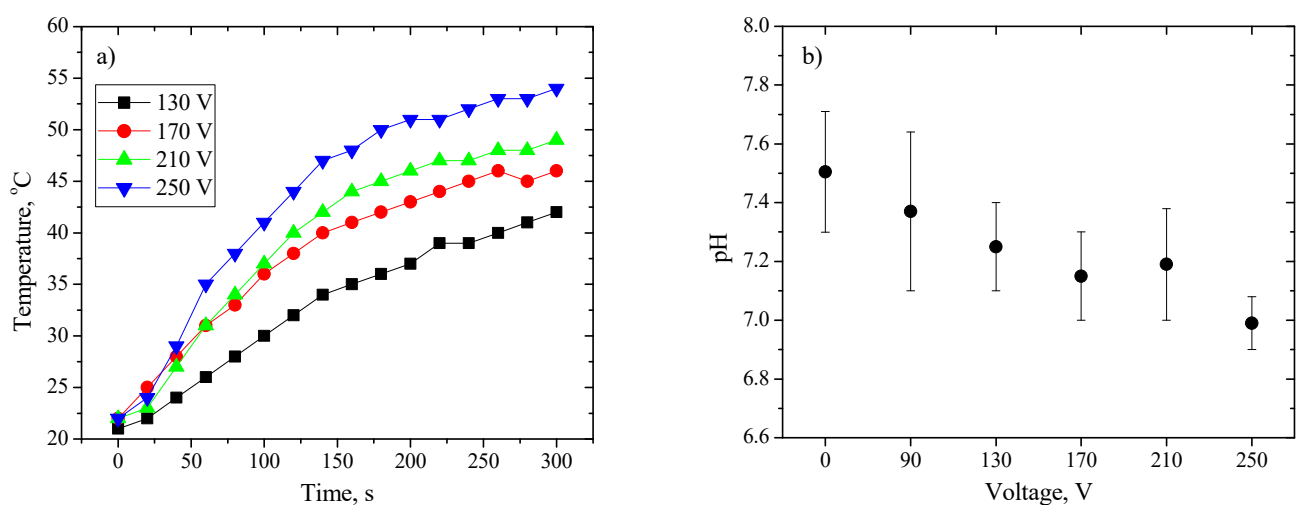
Figure 10. The dependence of the medium's temperature on the used voltage (**a**) and the variation its of pH values (**b**).

The effect of increasing the processing voltage was also observed in the medium's conductivity values (Figure 11a). The BG-11 medium, which initially had a conductivity of ~1.85 mS/cm, increased its conductivity after the air plasma treatment. The conductivity of the medium was 2.40 mS/cm when the treatment with air plasma was performed using 90 V. Meanwhile, the highest voltage (250 V) resulted in a significant increase in its conductivity, reaching 3.34 mS/cm—an 80% increase compared to the control medium (Figure 11a).
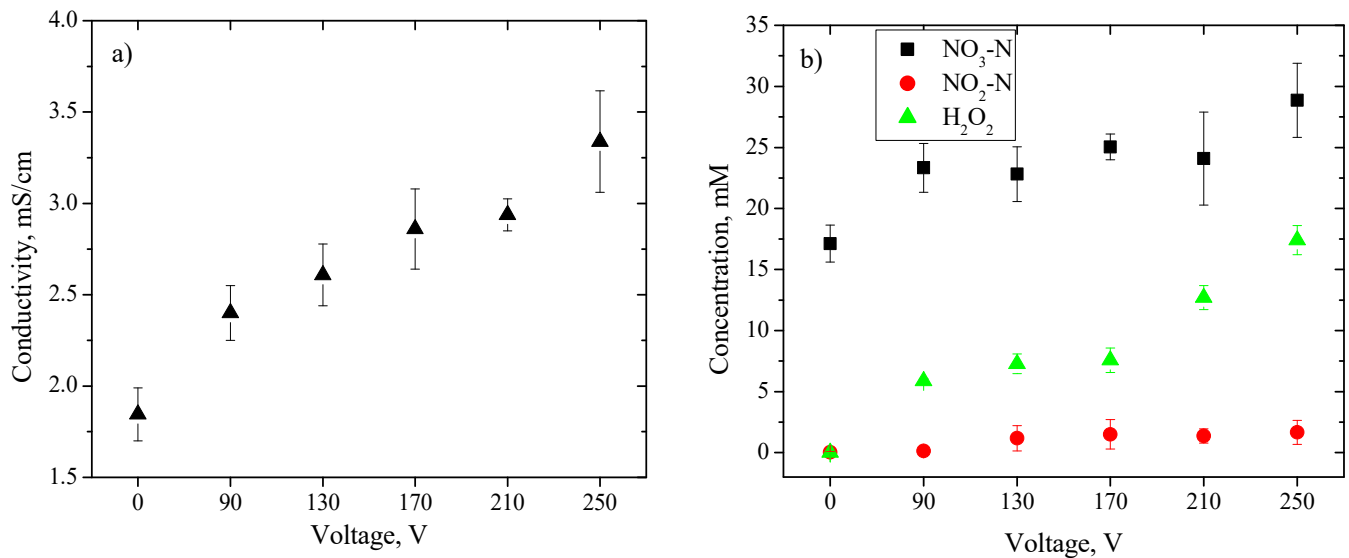
Figure 11. The variation of the conductivity (**a**) and concentration of nitrites, nitrates, and hydrogen peroxide (**b**) in liquid medium as a function of the output voltage.

The concentration of nitrites and nitrates in the liquid medium after the plasma treatment is given in Figure 11b. It can be seen that the NO_2^- concentration was enhanced from 0.13 mM to 1.67 mM with the increase in the voltage from 90 V to 250 V. The concentrations of NO_3^- were significantly higher compared to the concentrations of NO_2^- at similar voltages. However, a slight increase in the nitrates' concentrations from 23.3 mM to 28.9 mM was observed with the enhancement of the voltage. In addition to N radicals, the plasma treatment also induced the formation of hydrogen peroxide (H_2O_2), which was indirectly detected using the iodometric method. The concentration of hydrogen peroxide in the BG-11 medium after the plasma treatment with the lowest output voltage was ~5.9 mM. The concentration of H_2O_2 increased almost three times with an increase in the voltage to 250 V, resulting in about 17.4 mM (Figure 11b). The composition and abundances of the radicals produced by the plasma treatment in the BG-11 media are also confirmed by OES spectra, which showed an increase in the intensity of the N_2, N_2^+, O, and NO_γ lines with an increase in the discharge voltage (Figures 8 and 9). However, it is necessary to highlight that the levels of radicals detected, especially those of the N species, showed variability between replicates and fluctuated with time after the treatment (Figure 11b). Our analysis of the plasma's ability to generate radicals showed an increase of more than 50% in the nitrate concentration and a 4-fold increase in the nitrite concentration at the voltage of 250 V (Figure 11b).

V. Rathore et al. [6] observed that the conductivity of water increased, and the pH decreased, with the increase in the discharge power of the plasma. This effect was explained by the formation of higher concentrations of NO_2^- and NO_3^- ions in solutions or water when air plasma was used [6,43–45]. J. Pawlat et al. [21] observed that the concentration of nitrites and nitrates in water and deionized water were the highest when a mixture of N_2^+ 21% O_2 gases was used. Also, the conductivities of water and deionized water after their treatment with N_2, O_2, and N_2-O_2 plasma was increased. M. Gharagozalian et al. [45] observed that the nitrate concentration in water increased from 30 mg/L to ~70 mg/L after increasing the plasma treatment time from 2 min to 6 min. However, a further increase

in the plasma treatment time up to 16 min reduced the nitrate concentration down to 20 mg/L. This reduction in the NO_3^- concentration was attributed to the formation of HNO_3. The conductivity of tap water increased from 70 to 190 μS/cm and NO_3^- from 0.002 to 0.156 mmol/L after a 5 min air plasma treatment [43]. It was demonstrated that the pH values of water polluted with various bacteria decreased with an increase in the treatment time when using GAD plasma. The decrease in pH values was attributed to the formation of nitrite and nitrate ions, which, in water, are the acids HNO_3 and HNO_2, after plasma treatment [5]. It should be noted that the main species produced in various liquids, media, or water after plasma treatment are nitrites, nitrates, nitrogen dioxide, and hydrogen peroxide [4–6,8]. However, the concentrations of various species strongly depend on the type of water or media, type of plasma discharge, type of gases used, plasma treatment time, etc. [4–6,8,21,43–45].

In addition to the formation of HNO_3 acid after plasma treatment, the plasma generated NO species that are known to contribute to the formation of NO_x, which can subsequently hydrolyze to nitric and peroxonitric acids in liquids or waters [43,44]. An increase in the conductivity and concentration of nitrate and nitrite ions with voltage was observed (Figure 11b). This effect is due to the reactions of the NO_x species involved in the gas phase, liquid phase, and at the interface of the gas and liquid. The increase in voltage enhanced the concentration of the reactive species and radicals in air plasma, as the intensities of the emission lines were increased. Thus, a higher amount of these radicals and species will dissolve into the BG-11 medium during the plasma treatment and increase its concentration of nitrous and nitric acids and enhance its hydrogen peroxide fraction [6,8,43,44]. The increase in the concentration of the nitrite and nitrate ions will enhance the acidity and conductivity of the BG-11 medium. As a result, a more acidic medium with a higher conductivity value will be formed with an increase in the discharge voltage.

4. Conclusions

A gliding arc discharge plasma set-up was constructed, and the electrical characteristics of the air plasma discharge were investigated. It was revealed that the voltage and current waveforms of the discharge have a serrate-like shape, and that the increase in the output voltage has only a slight influence on the discharge voltage. Meanwhile, the highest arc current values near the discharge breakdown point were decreased from ~1.54 A to ~0.96 A with the increase in the voltage from 90 V to 250 V. It was observed that the increase in the voltage from 50 to 250 V increased the length of arc and enhanced the duration of the arc discharge from 1.71 ms up to 5.21 ms, respectively. The emission spectroscopy studies of the GAD air plasma indicated high-intensity N_2 lines, a moderate intensity of the N_2^+ and NO lines, and only a low intensity of the N^+ and O lines. The existence of only some traces of the emission lines of oxygen ions (O^+ and O_2^+) was confirmed. The increase in the voltage enhanced the ionization degree of the plasma and increased the densities of the N_2^+, N^+, O, and NO_γ species in the air plasma. The intensity of the emission lines of the O, NO_γ, and N_2^+ species was increased ~17, ~15, and ~8 times with the increase in V_G from 50 to 250 V. Meanwhile, the intensity of the emission lines attributed to excited N_2 particles was enhanced only ~3.5 times when this voltage was increased from 50 V to 170 V. A further increase in voltage resulted in a 10% reduction in the intensity of the N_2 emission lines.

The results indicated that the increase in the voltage lead to the production of a higher concentration of nitrite and nitrate ions and hydrogen peroxide in the BG-11 medium. The concentration of the hydrogen peroxide in the BG-11 medium was enhanced from 5.9 to 17.4 mM, the pH value was reduced from 7.37 to 6.99, and the conductivity of the medium was enhanced from 2.40 mS/cm to 3.34 mS/cm, when the voltage was increased from 90 V to 250 C, respectively. It should be noted that the conductivity of the medium was increased to almost double after the air plasma treatment. The performed studies indicated that by controlling the output voltage, it is possible to regulate the composition of the air plasma and produce a higher amount of NO species, which are important for the

application of GAD air plasma in the treatment of biological objects and for the creation of plasma-activated liquid or water.

Institutional Review Board Statement: Not applicable.

Informed Consent Statement: Not applicable.

Data Availability Statement: Data are contained within the article.

Conflicts of Interest: The authors declare no conflicts of interest.

References

1. Hertwig, C.; Meneses, N.; Mathys, A. Cold atmospheric pressure plasma and low energy electron beam as alternative nonthermal decontamination technologies for dry food surfaces: A review. *Trends Food Sci. Technol.* **2018**, *77*, 131–142. [CrossRef]
2. Beyrer, M.; Pina-Perez, M.C.; Martinet, D.; Andlauer, W. Cold plasma processing of powdered Spirulina algae for spore inactivation and preservation of bioactive compounds. *Food Control* **2020**, *118*, 107378. [CrossRef]
3. El-Sheekh, M.M.; Al-Halim, M.A.A.; Mohammed, S.A. Algae processing by plasma discharge technology: A review. *Algal Res.* **2023**, *70*, 102983. [CrossRef]
4. Choi, E.H.; Kaushik, N.K.; Hong, Y.J.; Lim, J.S.; Choi, J.S.; Han, I. Plasma bioscience for medicine, agriculture and hygiene applications. *J. Korean Phys. Soc.* **2022**, *80*, 817–851. [CrossRef]
5. Hameedl, T.A.; Kadhem, S.J. Gliding arc discharge for water treatment. *IOP Conf. Ser. Mater. Sci. Eng.* **2020**, *757*, 012045. [CrossRef]
6. Rathore, V.; Nema, S.K. Optimization of process parameters to generate plasma activated water and study of physicochemical properties of plasma activated solutions at optimum condition. *J. Appl. Phys.* **2021**, *129*, 084901. [CrossRef]
7. Mildažienė, V.; Ivankov, A.; Sera, B.; Baniulis, D. Biochemical and Physiological Plant Processes Affected by Seed Treatment with Non-Thermal Plasma. *Plants* **2022**, *11*, 856. [CrossRef]
8. Pipliya, S.; Kumar, S.; Babar, N.; Srivastav, P.P. Recent trends in non-thermal plasma and plasma activated water: Effect on quality attributes, mechanism of interaction and potential application in food & agriculture. *Food Chem. Adv.* **2023**, *2*. [CrossRef]
9. Rabinovich, A.; Nirenberg, G.; Kocagoz, S.; Surace, M.; Sales, C.; Fridman, A. Scaling Up of Non-Thermal Gliding Arc Plasma Systems for Industrial Applications. *Plasma Chem. Plasma Process.* **2021**, *42*, 35–50. [CrossRef]
10. Khani, M.R.; Shokri, B.; Khajeh, K. Studying the performance of dielectric barrier discharge and gliding arc plasma reactors in tomato peroxidase inactivation. *J. Food Eng.* **2017**, *197*, 107–112. [CrossRef]
11. Zhu, J.; Ehn, A.; Gao, J.; Kong, C.; Aldén, M.; Salewski, M.; Leipold, F.; Kusano, Y.; Li, Z. Translational, rotational, vibrational and electron temperatures of a gliding arc discharge. *Opt. Express* **2017**, *25*, 20243–20257. [CrossRef]
12. Ivanov, V.; Paunska, T.; Lazarova, S.; Bogaerts, A.; Kolev, S. Gliding arc/glow discharge for CO_2 conversion: Comparing the performance of different discharge configurations. *J. CO_2 Util.* **2023**, *67*. [CrossRef]
13. Ju, R.; Wang, J.; Zhang, M.; Mu, H.; Zhang, G.; Yu, J.; Huang, Z. Stability and emission characteristics of ammonia/air premixed swirling flames with rotating gliding arc discharge plasma. *Energy* **2023**, *277*. [CrossRef]
14. Liu, S.; Wang, B.; Cheng, Y.; Wang, C.; Zou, J. Ethanol partial oxidative reforming in gliding arc discharge plasma: A better understanding by a kinetic model study. *Fuel* **2022**, *328*, 125309. [CrossRef]
15. Mei, D.; Zhang, P.; Liu, S.; Ding, L.; Ma, Y.; Zhou, R.; Gu, H.; Fang, Z.; Cullen, P.J.; Tu, X. Highly efficient reforming of toluene to syngas in a gliding arc plasma reactor. *J. Energy Inst.* **2021**, *98*, 131–143. [CrossRef]
16. Choi, S.; Kang, H.; Kim, K.-T.; Song, Y.-H.; Lee, D.H. Ignition Process of Diesel Spray Based on Behavior of Rotating Gliding Arc in Plasma Reformer. *Plasma Chem. Plasma Process.* **2021**, *41*, 1021–1037. [CrossRef]
17. Guo, L.; Zhao, P.; Yao, Z.; Li, T.; Zhu, M.; Wang, Z.; Huang, L.; Niyazi, G.; Liu, D.; Rong, M. Inactivation of *Salmonella enteritidis* on the surface of eggs by air activated with gliding arc discharge plasma. *Food Control* **2023**, *148*, 109662. [CrossRef]

18. Dasan, B.G.; Onal-Ulusoy, B.; Pawlat, J.; Diatczyk, J.; Sen, Y.; Mutlu, M. A New and Simple Approach for Decontamination of Food Contact Surfaces with Gliding Arc Discharge Atmospheric Non-Thermal Plasma. *Food Bioprocess Technol.* **2017**, *10*, 650–661. [CrossRef]

19. Khalili, F.; Shokri, B.; Khani, M.-R.; Hasani, M.; Zandi, F.; Aliahmadi, A. A study of the effect of gliding arc non-thermal plasma on almonds decontamination. *AIP Adv.* **2018**, *8*. [CrossRef]

20. Ashtiani, S.-H.M.; Rafiee, M.; Morad, M.M.; Khojastehpour, M.; Khani, M.R.; Rohani, A.; Shokri, B.; Martynenko, A. Impact of gliding arc plasma pretreatment on drying efficiency and physicochemical properties of grape. *Innov. Food Sci. Emerg. Technol.* **2020**, *63*, 102381. [CrossRef]

21. Pawłat, J.; Terebun, P.; Kwiatkowski, M.; Tarabová, B.; Kovaľová, Z.; Kučerová, K.; Machala, Z.; Janda, M.; Hensel, K. Evaluation of Oxidative Species in Gaseous and Liquid Phase Generated by Mini-Gliding Arc Discharge. *Plasma Chem. Plasma Process.* **2019**, *39*, 627–642. [CrossRef]

22. Jelínek, P.; Polášková, K.; Jeník, F.; Jeníková, Z.; Dostál, L.; Dvořáková, E.; Cerman, J.; Šourková, H.; Buršíková, V.; Špatenka, P.; et al. Effects of additives on atmospheric pressure gliding arc applied to the modification of polypropylene. *Surf. Coat. Technol.* **2019**, *372*, 45. [CrossRef]

23. Kusano, Y.; Teodoru, S.; Leipold, F.; Andersen, T.L.; Sørensen, B.F.; Rozlosnik, N.; Michelsen, P.K. Gliding arc discharge—Application for adhesion improvement of fibre reinforced polyester composites. *Surf. Coat. Technol.* **2008**, *202*, 5579–5582. [CrossRef]

24. Sarkari, N.M.; Darvish, F.; Mohseni, M.; Ebrahimi, M.; Khani, M.; Eslami, E.; Shokri, B.; Alizadeh, M.; Dee, C.F. Surface characterization of an organosilane-grafted moisture-crosslinked polyethylene compound treated by air atmospheric pressure non-equilibrium gliding arc plasma. *Appl. Surf. Sci.* **2019**, *490*, 436–450. [CrossRef]

25. Kusano, Y.; Sørensen, B.F.; Andersen, T.L.; Toftegaard, H.L.; Leipold, F.; Salewski, M.; Sun, Z.; Zhu, J.; Li, Z.; Alden, M. Water-cooled non-thermal gliding arc for adhesion improvement of glass-fibre-reinforced polyester. *J. Phys. D: Appl. Phys.* **2013**, *46*, 135203. [CrossRef]

26. Dimitrakellis, P.; Faubert, F.; Wartel, M.; Gogolides, E.; Pellerin, S. Plasma Surface Modification of Epoxy Polymer in Air DBD and Gliding Arc. *Processes* **2022**, *10*, 104. [CrossRef]

27. Dhungana, S.; Guragain, R.P.; Baniya, H.B.; Panta, G.P.; Chhetri, G.K.; Subedi, D.P. Electrical and Optical Characterization of Gliding Arc Discharge (GAD) Operated at Line Frequency (50 Hz) Power Supply. *J. Nepal Phys. Soc.* **2020**, *6*, 26–33. [CrossRef]

28. Sun, Z.; Zhu, J.J.; Li, Z.; Aldén, M.; Leipold, F.; Salewski, M.; Kusano, Y. Optical diagnostics of a gliding arc. *Opt. Express* **2013**, *21*, 6028–6044. [CrossRef]

29. Aoqui, S.; Kawasaki, H.; Mitsugi, F.; Ohshima, T.; Sakai, E.; Muramoto, I.; Furukawa, J.; Stryczewska, H.D. Analysis of Gliding Arc Discharge Plasma Using a High-speed Camera and Emission Spectroscopy Measurement. In Proceedings of the 2nd International Symposium on Process Chemistry, Kyoto, Japan, 10–12 August 2011.

30. Ghabi, A.; Darny, T.; Dozias, S.; Bocanegra, P.E.; Pouvesle, J.-M.; Sarh, B.; Robert, E.; Boushaki, T. Effects of pulsed gliding arc plasma on non-premixed CH_4/CO_2–air flame stability. *Therm. Sci. Eng. Prog.* **2023**, *40*, 105024. [CrossRef]

31. Dimitrakellis, P.; Giannoglou, M.; Zeniou, A.; Gogolides, E.; Katsaros, G. Food container employing a cold atmospheric plasma source for prolonged preservation of plant and animal origin food products. *MethodsX* **2020**, *8*, 101177. [CrossRef]

32. Chen, G.C.; He, L.M.; Zhao, B.B.; Zhang, H.L.; Zhao, Z.C.; Zeng, H.; Lei, J.P.; Liu, X. Effects of Working Medium Gases on Emission Spectral and Temperature Characteristics of a Plasma Igniter. *Spectrosc.* **2019**, *2019*, 5395914. [CrossRef]

33. Wang, X.-Q.; Wang, F.-P.; Chen, W.; Huang, J.; Bazaka, K.; Ostrikov, K. Non-equilibrium plasma prevention of Schistosoma japonicum transmission. *Sci. Rep.* **2016**, *6*, 35353. [CrossRef]

34. Muzammil, I.; Lee, D.H.; Dinh, D.K.; Kang, H.; Roh, S.A.; Kim, Y.-N.; Choi, S.; Jung, C.; Song, Y.-H. A novel energy efficient path for nitrogen fixation using a non-thermal arc. *RSC Adv.* **2021**, *11*, 12729–12738. [CrossRef]

35. Parker, M. *Atmospheric Pressure Plasmas: Processes, Technology and Applications*; Nova Science Pub Inc.: Hauppauge, NY, USA, 2016; ISBN 978-1634851800.

36. U.C.C. of Algae. BG-11 Medium, UTEX Culture Collection of Algae. Available online: https://utex.org/products/bg-11-medium (accessed on 30 August 2023).

37. Putt, K.S.; Pugh, R.B. A High-Throughput Microtiter Plate Based Method for the Determination of Peracetic Acid and Hydrogen Peroxide. *PLoS ONE* **2013**, *8*, e79218. [CrossRef]

38. Zhang, R.; Huang, H.; Yang, T. Mode transition induced by back-breakdown of the gliding arc and its influence factors. *High Volt.* **2020**, *5*, 306–312. [CrossRef]

39. Machala, Z.; Janda, M.; Hensel, K.; Jedlovský, I.; Leštinská, L.; Foltin, V.; Martišovitš, V.; Morvová, M. Emission spectroscopy of atmospheric pressure plasmas for bio-medical and environmental applications. *J. Mol. Spectrosc.* **2007**, *243*, 194–201. [CrossRef]

40. Janda, M.; Martišovitš, V.; Hensel, K.; Machala, Z. Generation of Antimicrobial NOx by Atmospheric Air Transient Spark Discharge. *Plasma Chem. Plasma Process.* **2016**, *36*, 767–781. [CrossRef]

41. Wang, W.; Patil, B.; Heijkers, S.; Hessel, V.; Bogaerts, A. Nitrogen Fixation by Gliding Arc Plasma: Better Insight by Chemical Kinetics Modelling. *ChemSusChem* **2017**, *10*, 2145–2157. [CrossRef]

42. Rezaei, F.; Abbasi-Firouzjah, M.; Shokri, B. Investigation of antibacterial and wettability behaviours of plasma-modified PMMA films for application in ophthalmology. *J. Phys. D: Appl. Phys.* **2014**, *47*. [CrossRef]

43.   Mogo, J.P.K.; Fovo, J.D.; Sop-Tamo, B.; Mafouasson, H.N.A.; Ngwem, M.C.N.; Tebu, M.J.; Youbi, G.K.; Laminsi, S. Effect of Gliding Arc Plasma Activated Water (GAPAW) on Maize (*Zea mays* L.) Seed Germination and Growth. *Seeds* **2022**, *1*, 230–243. [CrossRef]

44.   Pandey, S.; Jangra, R.; Ahlawat, K.; Mishra, R.; Mishra, A.; Jangra, S.; Prakash, R. Selective generation of nitrate and nitrite in plasma activated water and its physicochemical parameters analysis. *Phys. Lett. A* **2023**, *474*, 128832. [CrossRef]

45.   Gharagozalian, M.; Dorranian, D.; Ghoranneviss, M. Water treatment by the AC gliding arc air plasma. *J. Theor. Appl. Phys.* **2017**, *11*, 171–180. [CrossRef]